Dichlorinated Organic-Salt Terahertz Sources for THz Spectroscopy

Bong-Rim Shin†, *In Cheol Yu*†, *Mojca Jazbinsek, Woojin Yoon, Hoseop Yun, Sang-Wook Kim, Dongwook Kim, Fabian Rotermund*, O-Pil Kwon**

((Optional Dedication))

B. R. Shin, Prof. S. W. Kim, Prof. O. P. Kwon
Department of Molecular Science and Technology, Ajou University, Suwon 16499 (Korea)
E-mail: opilkwon@ajou.ac.kr
I. C. Yu, Prof. F. Rotermund
Department of Physics, Korea Advanced Institute of Science and Technology (KAIST), Daejeon 34141 (Korea)
E-mail: rotermund@kaist.ac.kr
Dr. M. Jazbinsek
Institute of Computational Physics, Zurich University of Applied Sciences (ZHAW), 8401 Winterthur (Switzerland)
W. Yoon, Prof. H. Yun
Department of Chemistry & Department of Energy Systems Research, Ajou University, Suwon 16499 (Korea)
Prof. D. Kim
Department of Chemistry, Kyonggi University, San 94-6, Iui-dong, Yeongtong-gu, Suwonsi, Gyeonggi 443-760 (Korea)

†These authors equally contributed to this work.

Keywords: terahertz waves; self-assembly, organic crystals; nonlinear optics; halogen bonds

Abstract:

We report new organic-salt dichlorinated crystals acting as excellent coherent terahertz (THz) sources. Although in THz source materials molecular anions significantly influence on the performance of THz generation, only limited classes of molecular counter anions have been reported. Utilizing dichlorinated molecular anions in THz generators is reported for the first time, to the best of our knowledge. In these new crystals, two dichlorinated molecular anions with different molecular symmetries, asymmetric 3,4-dichlorobenzenesulfonate (34DCS) and symmetric 3,5-dichlorobenzenesulfonate (35DCS), are incorporated with a 2-(4-hydroxystyryl)-1-methylquinolinium (OHQ) cation possessing top-level molecular optical nonlinearity. OHQ-34DCS exhibits a strong nonlinear optical response, in contrast to OHQ-35DCS. In OHQ-34DCS crystals, the dichlorinated groups form strong halogen bonds (XBs) and hydrogen bonds (HBs), which are beneficial for suppressing molecular (phonon) vibrations. The optical-to-THz conversion efficiency of the OHQ-34DCS crystals is extremely high, comparable to that of the benchmark organic THz generators. Moreover, the THz emission spectra from the OHQ-34DCS crystals, compared to those of previously reported benchmark analogous crystals, are stronger modulated toward a flatter shape, but possess substantially reduced spectral dimples. Therefore, the introduction of dichlorinated molecular anions is an efficient approach for the design of highly efficient electro-optic salt crystals as efficient broadband THz wave sources.

1. Introduction

Terahertz (THz) waves are widely applied in various fundamental and applied research areas, such as spectroscopy, imaging, sensing, pump and/or probe experiments, and spin (and magnetic) control of matter.[1-6] In the current THz photonics field, the development of efficient and broadband sources of electromagnetic waves at THz frequencies is a crucial issue, which is sometimes referred to as the THz gap due to the scarcity of such sources.[7,8] Therefore, many studies have attempted to address this unfavorable situation by developing efficient and/or broadband THz wave sources based on fundamental approaches such as nonlinear optics, photoconductivity, gas plasmas, and spintronics.[3,8-10]

Among various THz source materials, organic electro-optic salt crystals have shown excellent potential for efficient THz wave generation, as they simultaneously achieve high generation efficiency and broad spectral bandwidth even in table-top setups and simple collinear geometries.[3,10] In the last two decades, various new organic electro-optic salt crystals have been designed for THz wave generation.[11-20] In addition, organic electro-optic salt crystals reported before the year 2000 have been recently examined for performance of THz wave generation and THz wave-related activity.[21-26] Many organic electro-optic salt crystals have top-level nonlinear optical coefficients. For example, organic salt crystals possessing effective first hyperpolarizability of $> 100 \times 10^{-30}$ esu show very high conversion efficiency in THz wave generation, mostly providing over 10 times higher amplitude than that of inorganic semiconducting crystals when pumped at infrared optical wavelengths.[10]

Through analyses of the chemical structure of benchmark organic salt THz sources, versatile classes of cationic chromophores have been discovered.[10,27-29] However, there are only limited classes of molecular counter anions. Mono-substituted benzenesulfonate anions have been used in several benchmark organic salt crystals. For example, non-polar methyl group was introduced for mono-substituent on the benzenesulfonate anion in pyridinium-based 4-(4-(*N,N*-dimethylamino)styryl)-1-methylpyridinium 4-methylbenzenesulfonate (DAST), quinolinium-based

2-(4-hydroxystyryl)-1-methylquinolinium 4-methylbenzenesulfonate (OHQ-T), benzothiazolium-based 2-(4-hydroxy-3,5-dimethylstyryl)-3-methylbenzothiazol-3-ium 4-methylbenzenesulfonate (HDB-T), and indolium-based 2-(4-hydroxystyryl)-1,3,3-trimethyl-3H-indolium 4-methylbenzenesulfonate (OHI-T) crystals.[11-13,21] A polar nitro group was introduced for mono-substituent on the benzenesulfonate anion in indolium-based 1-ethyl-2-(4-(4-(hydroxymethyl)piperidin-1-yl)styryl)-3,3-dimethyl-3H-indolium 4-nitrobenzenesulfonate (EHPSI-4NBS) crystals.[14] Furthermore, a polar trifluoromethoxy group was introduced for mono-substituent on the benzenesulfonate anion in benzothiazolium-based 2-(4-hydroxystyryl)-3-methylbenzothiazol-3-ium 4-(trifluoromethoxy)benzenesulfonate (OHB-TFO).[15]

Although molecular counter anions show a negligibly small contribution to the macroscopic optical nonlinearity in crystals, the intermolecular interactions induced by molecular anions significantly influence the characteristics of THz wave generation (e.g., generation efficiency, spectral bandwidth, spectral shape and flatness, and self-absorption).[10,30,31] Consequently, in organic salt THz source materials, the selection of molecular anions contributed crucially.

The use of previously unreported molecular anions for developing new organic salt THz source materials is challenging. To achieve a top-level THz generation efficiency comparable to that of benchmark organic-salt THz sources, when new molecular anions are introduced, the macroscopic optical nonlinearity of the crystals must exceed 100×10^{-30} esu.[10] However, the introduction of unreported molecular anions into new crystals in most cases does not lead to desired molecular packing and intermolecular interactions, which deteriorates the macroscopic optical nonlinearity and thus hinders THz wave generation.

In this work, we report new organic-salt THz source crystals containing dichlorinated molecular anions for the first time. The introduction of dichlorinated benzenesulfonate anions to organic salt crystals yields top-level macroscopic optical nonlinearity (effective first hyperpolarizability of 119×10^{-30} esu), leading to state-of-the-art optical-to-THz conversion efficiency. In particular, the THz emission spectra of the new dichlorinated crystals are stronger modulated toward a flatter shape, but

possess substantially reduced spectral dimples compared to those of previously reported analogous crystals. In the crystals, the dichlorinated groups on the anions participate in strong intermolecular interactions with both strong halogen and hydrogen bonds. Therefore, the introduction of dichlorinated molecular anions is an attractive approach for use in organic-salt THz sources.

2. Results and Discussion

2.1. Design of Dichlorinated Organic Salt Crystals

In organic THz source materials, intermolecular interactions related to molecular phonon vibrations (i.e., optical characteristic features in the THz frequency range) significantly influence the characteristics of THz wave generation.[30-33] Recently, halogen bonds (XBs) have attracted considerable attention owing to their effects on intermolecular interactions in organic π-conjugated crystals. The introduction of halogen substituents on π-conjugated groups, as shown with the Cl substituent in Figure 1a, can simultaneously form XBs and hydrogen bonds (HBs) in different directions.[34,35] Compared to conventional non-polar and polar substituents that can form only weak and strong HBs, respectively, the positive σ-hole and negative belt on the halogen substituent can yield multi-intermolecular interactions with both XBs and HBs.

In this work, for designing organic electro-optic crystals that act as efficient THz sources, dichlorinated substituents are added to molecular anions. To visualize the multi-intermolecular interaction ability (XBs and HBs) of dichlorinated substituents on the aromatic ring, the electrostatic potentials of 1,2- and 1,3-dichlorobenezenes (DCB) were calculated by density functional theory (DFT) using the B3LYP/6-311+G(d,p) basis set. The results are shown in Figure 1b. The coexisting positive σ-hole and negative belt on the Cl substituents on the aromatic ring are clearly visible. The possible multi-intermolecular interactions (XBs and HBs) of dichlorinated substituents (Figure 1b) with other substituents used in many organic THz source crystals are illustrated in Figure S1. For

example, the positive σ-hole (δ+) and the negative belt (δ-) on Cl substituents can form XBs with (δ-) sulfonate groups and HBs with (δ+) H-Ar groups, respectively.

Figure 1c shows the chemical structure of the newly designed organic-salt THz source crystals. Here, the two dichlorinated molecular anions have different molecular symmetries: 3,4-dichlorobenzenesulfonate (34DCS) is asymmetric, whereas 3,5-dichlorobenzenesulfonate (35DCS) is symmetric. The symmetry of the molecular components of organic crystals is one of the important parameters for achieving non-centrosymmetric molecular ordering in the crystalline state. For nonlinear optical chromophores, the symmetry reduction of the molecular shape can help to achieve the non-centrosymmetric ordering of chromophores in crystals.[27]

As a nonlinear optical chromophore, the 2-(4-hydroxystyryl)-1-methylquinolinium (OHQ) cation with a large maximum first hyperpolarizability β_{max} in the gas phase (118×10^{-30} esu)[11] was used in this work. The newly designed dichlorinated OHQ-34DCS and OHQ-35DCS were synthesized by a condensation reaction in a manner similar to that reported in the literature.[11,16]

Thermal analysis of OHQ-34DCS and OHQ-35DCS was performed to investigate whether the introduction of dichlorinated substituents to organic salt crystals affects the thermal stability, since it is important for the allowed range of operating temperatures and stability of THz sources. Figure S2a and S1b show the thermogravimetric analysis (TGA) and differential scanning calorimetry (DSC) thermodiagrams of OHQ-34DCS and OHQ-35DCS, respectively. For both compounds, the melting temperature T_m and the initial weight loss temperature T_i are sufficiently high, above 240 °C. The introduction of dichlorinated substituents thus does not harm the thermal stability within the operating temperature of widely used THz sources. The melting temperature T_m of OHQ-34DCS (258 °C) is higher than that of OHQ-35DCS. In powder second harmonic generation (SHG) measurements[36,37] with pumping at 1300 nm, OHQ-34DCS exhibited a nonlinear optical response with a strong SHG signal, while OHQ-35DCS did not show an SHG signal (Figure S2c). This shows that OHQ-34DCS crystals with the asymmetric anion 34DCS possess a desired acentric chromophore alignment, while the chromophore alignment in OHQ-35DCS crystals with the symmetric anion 35DCS possesses a

centrosymmetric symmetry or very close to it. Consequently, OHQ-34DCS with the potential for nonlinear optical applications such as efficient THz wave generation was further investigated in detail.

2.2. Crystal Characteristics for THz Sources

To perform X-ray single crystal structure analysis, OHQ-34DCS single crystals are grown by cooling method in a mixed solvent of methanol and acetonitrile. OHQ-34DCS single crystals exhibit triclinic *P1* space-group symmetry with one molecular pair (one cation and one anion) in the unit cell. Figure 2a and 2b show the molecular ordering of the OHQ cations and 34DCS anions in the crystalline state. In the OHQ-34DCS crystals, the nonlinear optical OHQ cations are aligned perfectly parallel with non-centrosymmetric ordering. The OHQ cations possess very planar conformation (Figure 2b) that is helpful for efficient π-electron delocalization (i.e., not deteriorate first hyperpolarizability of OHQ cations).

To investigate the details of the nonlinear optical characteristics of OHQ-34DCS crystals, which are important for THz wave generation, the maximum first hyperpolarizability β_{max} of the OHQ cation was calculated by DFT calculations using the B3LYP/6-311+G(d,p) basis set.[38,39] The theoretical maximum first hyperpolarizability β_{max} value for the OHQ cation having experimental conformation (EXP) in OHQ-34DCS crystals is very large; 119×10^{-30} esu (see details in Supporting Information, Section E). The corresponding direction of maximum first hyperpolarizability β_{max} of the OHQ cation in the OHQ-34DCS crystal is indicated by the red arrow in Figure 3a. The polar axis of OHQ-34DCS crystal, represented by the blue dotted arrow, is exactly parallel to the direction of the maximum first hyperpolarizability β_{max} of the OHQ cation, which is because of the *P*1 symmetry with only one chromophore per unit cell. For the same reason, the macroscopic nonlinear optical coefficient (diagonal effective first hyperpolarizability for the OHQ-34DCS crystal) is also very large and equal to the value of the maximum first hyperpolarizability: $\beta_{111}^{eff} = \beta_{max} = 119 \times 10^{-30}$ esu. Therefore, the

introduction of dichlorinated asymmetric molecular anions resulted in top-level macroscopic optical nonlinearity (> 100 × 10^{-30} esu), comparable to that of benchmark organic-salt THz sources.

In OHQ-34DCS crystals, strong intermolecular interactions were observed. In Figure 2c, the red dotted lines indicate many strong intermolecular interactions with the short-distance all···all atom contacts (< 3.0 Å) observed in the Hirshfeld surface analysis.[40-42] In particular, the dichlorinated substituents form strong XBs and HBs in crystals as illustrated in Figure S1. As shown in Figure 1d, the Cl substituents on the 34DCS anion in the OHQ-34DCS crystal form two strong XBs between anions ((Ar)–Cl(δ+)···$^{-}O_3$–S–) with very short distances of 2.94 and 3.33 Å. Figures 4a and 4b show that the intermolecular interactions of OHQ-34DCS crystals include HBs between Cl and H with the close contact of Cl···H and H···Cl (< 3.0 Å) on the Hirshfeld surface. These intermolecular interactions of the OHQ-34DCS crystals (i.e., both XBs and HBs in Figure 1d and Figure 4a and 4b, respectively) with dichlorinated molecular anions (34DCS) do not exist in previously reported analogous, but OHQ-T crystals[11] with mono-substituted (non-chlorinated methyl) molecular anions (4-methylbenzenesulfonate (T)).

The crystal density of the OHQ-34DCS crystals (1.481 g/cm^3) is remarkably higher than that of OHQ-T crystals (1.351 g/cm^3). The volume of the unit cell per one cation-anion pair is for OHQ-34DCS crystals (~548 $Å^3$) with larger substituents slightly larger than for OHQ-T crystals (~533 $Å^3$). The higher density in OHQ-34DCS crystals compared to OHQ-T crystals results from the higher mass in the unit cell; i.e., introducing heavy dichlorinated substituent with 70.9 g/mol instead of methyl substituent with 15.0 g/mol. The higher density of OHQ-34DCS crystals is attributed to the relatively strong interactions induced by dichlorinated substituent (Hirshfeld fingerprints in Figure 1d and Figure 4a-b for XBs and HBs, respectively).

In addition to the higher density, the void volume[43] of the OHQ-34DCS crystals (27.9 %) is slightly lower than that of OHQ-T crystals (28.5 %).[44] Figure 1e shows a part of the void shape around the dichlorinated substituent on 34DCS anions in OHQ-34DCS crystals. The areas around

multi-intermolecular interactions of dichlorinated substituents - XBs between (Ar)–Cl(δ+)···$^{-}O_3S$– groups, presented with red dotted lines in Figure 1e and Hirshfeld fingerprints in Figure 1d – are corresponding to non-void areas.

Consequently, compared to previously reported OHQ-T crystals, OHQ-34DCS crystals with dichlorinated substituent on anions exhibit additional intermolecular interactions, higher crystal density, and lower void volume. Many molecular vibrational motions of molecular anions result in absorption of organic salts in the THz frequency range, which limits their efficiency when used as THz sources.[10,30,31] Due to stronger intermolecular interactions, higher density and lower void volume compared to previously reported OHQ-T crystals, OHQ-34DCS crystals may have weaker molecular vibrational motions of 34DCS molecular anions compared to T anions in OHQ-T crystals. Therefore, introducing dichlorinated substituent on molecular anions that results in additional intermolecular interactions, higher crystal density, and lower void volume is an efficient approach for obtaining weaker molecular vibrational motions, which is favorable for THz source crystals.

In bulk crystal growth experiments using a mixed solvent of methanol and acetonitrile, two morphologies of OHQ-34DCS crystals were concomitantly obtained. Figure 3b and 3c show the photographs of OHQ-34DCS crystals with different morphologies having in-plane and (close-to) out-of-plane polar axis, respectively. The largest surface of OHQ-34DCS crystals with morphology as in Figure 3b is the crystallographic (001) plane that was determined by reflection X-ray diffraction measurement. The direction of the polar axis is rotated by only about 6.2-degree with respect to the crystallographic *ab* or (001) plane as shown in Figure 3a. The long molecular axis of OHQ cations and approximately also 34DCS anions is parallel with the direction of the polar axis. Due to the high difference in the polarizability along and perpendicular to the long axis of these molecules, we expect a high anisotropy and a large birefringence of these crystals, which is confirmed by observing these crystals between crossed polarizers. The direction of the polar axis in the OHQ-34DCS crystals was determined by a polarizer. The OHQ-34DCS crystals with an in-plane polar axis exhibit a very strong birefringence and an easily observable shift of the absorption edge (different color, see Figure 3b) for

the two in-plane eigen polarizations. When the color of OHQ-34DCS crystals in transmission is the darkest (right photograph in Figure 3b), the light polarization direction is parallel with the direction of the polar axis with a higher refractive index and the associated red-shifted absorption edge. On the other hand, the crystals with a morphology like shown in Figure 3c do not show a strong anisotropy, therefore the polar axis must be oriented close to the normal direction (out-of-plane). Considering the ordering of the OHQ cation (i.e., the direction of the polar axis) and the (001) facet of the as-grown OHQ-34DCS crystals, OHQ-34DCS crystals with an in-plane polar axis are highly suitable for THz wave generation in a simple collinear geometry (Figure 3d).

2.3. Efficient THz Wave Generation

For efficient THz wave generation, an OHQ-34DCS crystal with an in-plane polar axis was pumped by 130-fs optical pulses at 1-kHz repetition rate. The incident angle of the optical pump was normal to the crystallographic (001) plane of the OHQ-34DCS crystal, as shown in Figure 3d. The details of our experimental setup is additionally shown in Figure S4 of Supporting Information. Pump wavelengths of 1140 and 1300 nm were selected for comparison. The electro-optic sampling (EOS) technique with a 0.3-mm <110> GaP crystal and probe pulses at 800 nm was used for detection.

The THz wave generation efficiency of the OHQ-34DCS crystals was evaluated based on a comparison with widely used, commercially available inorganic standard crystals (ZnTe) with a thickness of 1.0 mm. Figure 3e and 3f show the THz wave generation results from a 0.48-mm-thick OHQ-34DCS crystal pumped at 1140 and 1300 nm. The 0.48-mm-thick OHQ-34DCS crystal exhibited high optical-to-THz conversion efficiency; the peak-to-peak THz electric field of the OHQ-34DCS crystal was 20 times higher than that of the 1.0-mm-thick ZnTe crystal at 1300 nm (Figure 3e). The resulting spectral bandwidth of the OHQ-34DCS crystal was much broader than that of the ZnTe crystal (Figure 3e). To provide more information on THz wave generation characteristics, the THz field strength was measured as a function of the optical pump power in the power level from 6 to 18 mW (corresponding to intensities of 47 to 140 GW/cm^2). Up to 10-mW pump power, the THz

field increases linearly with the pump power and starts to slightly saturate above 10 mW. Nevertheless, the OHQ-34DCS crystal provides very stable THz emission performance without any specific thermal fluctuation and drift. The results of the pump-power-dependent THz wave generation are summarized in Figure S5. Note that in organic THz crystals having orange-color; i.e., absorption edge in visible wavelength (e.g., OHQ-T), THz generation stability is not crucial issue when pumped at infrared wavelength.[10] Since OHQ-34DCS crystals consist of identical orange-color OHQ cations with OHQ-T crystals, the OHQ-34DCS crystal exhibits excellent THz generation stability in our experiment. Consequently, the newly designed OHQ-34DCS single crystals are highly promising THz source materials.

Note that the resulting spectral bandwidth of OHQ-34DCS crystals may be limited by other optical experimental conditions, e.g., pulse duration of optical pump (130-fs here). In many organic THz source crystals pumped at good phase-matchable infrared wavelengths of ≥ 1000 nm, using shorter pump pulses results in increasing the spectral bandwidth that is accompanied with the change of the generated spectral shape. In addition, the generated THz spectral bandwidth and shape are also varied with extrinsic material parameters; e.g., thickness of THz source crystals.[10] Therefore, the THz wave generation performance of OHQ-34DCS crystals may be further improved by changing the optical experimental conditions and extrinsic material parameters.

In addition, the THz wave generation performance of OHQ-34DCS crystals was compared with that of a top-level THz source, i.e., OHQ-T crystals, which are analogous to OHQ-34DCS crystals, but based on mono-substituted benzenesulfonate anions. As shown in Figure 4c, the THz conversion efficiency of the OHQ-34DCS crystals was similar to that of OHQ-T crystals of a similar thickness. This is related to the similar macroscopic optical nonlinearity of OHQ-34DCS and OHQ-T crystals; $\beta_{111}^{\mathrm{eff}} = 119 \times 10^{-30}$ and 121×10^{-30} esu[11], respectively.

Interestingly, although the OHQ-34DCS crystals exhibited a THz conversion efficiency similar to that of the OHQ-T crystals with an almost identical thickness (Figure 4c), the shape of the THz spectra substantially differed. As shown in Figure 4d, the THz emission spectra of the OHQ-34DCS

crystals were stronger modulated toward a flatter shape compared to those of the OHQ-T crystals. While OHQ-T exhibits a very broad spectral dimple at around 1.5 THz, OHQ-34DCS shows additional spectral content in this region with substantially reduced spectral dimples. This flatter spectral shape of the OHQ-34DCS crystals is beneficial for various THz applications including spectroscopy.

The spectral dimples generated from OHQ-34DCS crystals are strongly correlated to the absorption characteristics in THz frequency range. Figure S6 shows the absorbance of a 0.48-mm-thick OHQ-34DCS crystal in the THz frequency range, with a systematic absorbance limit calculated from the dynamic range of a reference THz field. While OHQ-T crystals exhibit a very strong and broad absorption peak at around 1.5 THz,[11] OHQ-34DCS crystals show relatively sharp absorption peaks around 1.1, 1.6 and 2.2 THz with a rather broad peak at 3.2 THz. In both OHQ-34DCS and OHQ-T crystals, the absorption peak position is superimposed with the dimple position in the generated THz spectra (Figure 4d).

The difference in THz spectral shapes with different dimples (and absorption) is attributed to the different intermolecular interaction characteristics of the two crystals. As shown in Figure S3, the overall face-to-face and edge-to-face π–π interactions of the OHQ-34DCS crystals are similar to those of OHQ-T crystals. However, as described above, OHQ-34DCS crystals exhibit additional intermolecular interactions induced by the dichlorinated substituents (XBs in Figure 1d and HBs in Figure 4a and 4b), as well as lower void volume and higher crystal density than OHQ-T crystals. Therefore, in OHQ-34DCS crystals the molecular vibrational motions are better suppressed compared to OHQ-T crystals with a standard counter anion, which leads to a reduced self-absorption of the generated THz waves. In another quinolinium-based and pyridinium-based organic-salt THz sources, it was shown that below and around 2 THz, the phonon resonances involve entire molecular motions (i.e., entire molecular rotations and translations) of both cations and anions.[31-33] The introduction of 34DCS anions with dichlorinated substituents may result in a reduction in these entire molecular

phonon motions, leading to a flatter shape of the THz emission spectra below (and around) 2 THz, as shown in Figure 4d.

3. Conclusion

To the best of our knowledge, this is the first report of a highly efficient electro-optic salt crystals utilizing dichlorinated aromatic molecular anions. OHQ-34DCS crystals exhibit top-level macroscopic optical nonlinearity, leading to state-of-the-art optical-to-THz conversion efficiency. The introduction of dichlorinated molecular anions into organic salt crystals is an efficient approach for achieving both a flat spectral shape and high conversion efficiency in THz wave generation because the dichlorinated groups that form XBs and HBs. Therefore, the use of dichlorinated molecular anions is a highly useful strategy for the design of organic salt electro-optic and THz source crystals.

4. Experimental Section

The details of the synthesis of OHQ-34DCS and OHQ-35DCS, thermal analysis, powder SHG measurements, crystal structure analysis, and intermolecular interaction analysis are provided in the Supporting Information.

Supporting Information

Supporting Information is available from the Wiley Online Library or from the author.

Acknowledgements

B. R. S. and I. C. Y contributed equally to this work. This work has been supported by the National Research Foundation of Korea (NRF) funded by the Ministry of Science, ICT & Future Planning, Korea (No. 2021R1A2C1005012, 2021R1A5A6002853, 2019K1A3A1A14057973, 2019R1A2C3003504), Institute of Information & communications Technology Planning & Evaluation (IITP) grant funded by the Korea government (MSIT) (No. 2022-0-00624) and Swiss National Science Foundation (SNSF), Switzerland (No. IZKSZ2_188194). X-ray structural analysis was supported by Basic Science Research Program through the National Research Foundation of Korea (NRF) funded by the Ministry of Education (2019R1I1A2A01058066).

Received: ((will be filled in by the editorial staff))
Revised: ((will be filled in by the editorial staff))
Published online: ((will be filled in by the editorial staff))

References

[1] T. Kampfrath, K. Tanaka, K. Nelson, *Nat. Photonics* **2013**, *7*, 680.

[2] S. Fratini, M. Nikolka, A. Salleo, G. Schweicher, H. Sirringhaus, *Nat. Mater.* **2020**, *19*, 491.

[3] J. A. Fülöp, S. Tzortzakis, T. Kampfrath, *Adv. Opt. Mater*. **2020**, *8*, 1900681.

[4] X. Chen, D. Hu, R. Mescall, G. You, D. Basov, Q. Dai, M. Liu, *Adv. Mater.* **2019**, *31*, 1804774.

[5] F. Perakis, L. D. Marco, A. Shalit, F. Tang, Z. R. Kann, T. D. Kühne, R. Torre, M. Bonn, Y. Nagata, *Chem. Rev*. **2016**, *116*, 7590.

[6] Y. Roh, S.-H. Lee, J. Kwak, H. S. Song, S. Shin, Y. K. Kim, J. W. Wu, B.-K. Ju, B. Kang, M. Seo, *Sens. Actuators, B* **2022**, *352*, 130993.

[7] C. Sirtori, *Nature* **2002**, *417*, 132.

[8] M. Tonouchi, *Nat. Photon*. **2007**, *1*, 97.

[9] H. A. Hafez, X. Chai, A. Ibrahim, S. Mondal, D. Férachou, X. Ropagnol, T. Ozaki, *J. Opt.* **2016**, *18*, 093004.

[10] S. J. Kim, B. J. Kang, U. Puc, W. T. Kim, M. Jazbinsek, F. Rotermund, O. P. Kwon, *Adv. Opt. Mater*. **2021**, *9*, 2101019.

[11] S. H. Lee, B. J. Kang, J. S. Kim, B. W. Yoo, J. H. Jeong, K. H. Lee, M. Jazbinsek, J. W. Kim, H. Yun, J. Kim, Y. S. Lee, F. Rotermund, O. P. Kwon, *Adv. Opt. Mater.* **2015**, *3*, 756.

[12] J. Shi, F. Liang, Y. He, X. Zhang, Z. Lin, D. Xu, Z. Hu, J. Yao, Y. Wu, *Chem. Commun.* **2019**, *55*, 7950.

[13] J. Shi, Y. He, F. Liang, X. Zhang, D. Xu, J. Yao, G. Zhang, Z. Hu, J. Yao, Y. Wu, J. *Mater. Chem. C* **2020**, *8*, 4226.

[14] G. A. Valdivia-Berroeta, E. W. Jackson, K. C. Kenney, A. X. Wayment, I. C. Tangen, C. B. Bahr, S. J. Smith, D. J. Michaelis, J. A. Johnson, *Adv. Funct. Mater.* **2020**, *30*, 1904786.

[15] M. H. Shin, W. T. Kim, S. I. Kim, S. J. Kim, I. C. Yu, S. W. Kim, M. Jazbinsek, W. Yoon, H. Yun, F. Rotermund, O. P. Kwon, *Adv. Sci.* **2020**, *7*, 2001738.

[16] P. J. Kim, J. H. Jeong, M. Jazbinsek, S. B. Choi, I. H. Baek, J. T. Kim, F. Rotermund, H. Yun, Y. S. Lee, P. Günter, O. P. Kwon, *Adv. Funct. Mater.* **2012**, *22*, 200.

[17] a) Z. Yang, L. Mutter, M. Stillhart, B. Ruiz, S. Aravazhi, M. Jazbinsek, A. Schneider, V. Gramlich, P. Günter, *Adv. Funct. Mater.* **2007**, *17*, 2018; b) M. Savoini, L. Huber, H. Cuppen, E.

Abreu, M. Kubli, M. J. Neugebauer, Y. Duan, P. Beaud, J. Xu, T. Rasing, S. L. Johnson, *ACS Photonics* **2018**, *5*, 671; c) R. Shi, X. Han, P. Cheng, M. Xin, J. Xu, *Cryst. Growth Des*. **2022**, *22*, 3998; d) G. A. Valdivia-Berroeta, Z. B. Zaccardi, S. K. F. Pettit, S. H. Ho, B. W. Palmer, M. J. Lutz, C. Rader, B. P. Hunter, N. K. Green, C. Barlow, C. Z. Wayment, D. J. Ludlow, P. Petersen, S. J. Smith, D. J. Michaelis, J. A. Johnson, *Adv. Mater*. **2022**, *34*, 2107900.

[18] C. U. Jeong, B. J. Kang, S. H. Lee, S. C. Lee, W. T. Kim, M. Jazbinsek, W. Yoon, H. Yun, D. Kim, F. Rotermund, O. P. Kwon, *Adv. Funct. Mater.* **2018**, *28*, 1801143.

[19] S. H. Lee, J. Lu, S. J. Lee, J. H. Han, C. U. Jeong, S. C. Lee, X. Li, M. Jazbinšek, W. Yoon, H. Yun, B. J. Kang, F. Rotermund, K. A. Nelson, O. P. Kwon, *Adv. Mater.* **2017**, *29*, 1701748.

[20] J. H. Seok, D. Kim, W. T. Kim, S. J. Kim, W. Yoon, G. E. Yoon, I. C. Yu, M. Jazbinsek, S. W. Kim, H. Yun, D. Kim, F. Rotermund, O. P. Kwon, *Adv. Opt. Mater.* **2021**, *9*, 2100324.

[21] S. R. Marder, J. W. Perry, W. P. Schaefer, *Science* **1989**, *245*, 626.

[22] S. R. Marder, J. W. Perry, C. P. Yakymyshyn, *Chem. Mater.* **1994**, *6*, 1137.

[23] I. Katayama, R. Akai, M. Bito, H. Shimosato, K. Miyamoto, H. Ito, M. Ashida, *Appl. Phys. Lett.* **2010**, *97*, 021105.

[24] S. R. Tripathi, K. Murate, H. Uchida, K. Takeya, K. Kawase, *Appl. Phys. Express* **2013**, *6*, 072703.

[25] M. Tang, H. Minamide, Y. Wang, T. Notake, S. Ohno, H. Ito, *Opt. Express* **2011**, *19*, 779.

[26] a) T. Notake, K. Nawata, H. Kawamata, T. Matsukawa, F. Qi, H. Minamide, *Opt. Express* **2012**, *20*, 25850; b) K. Fan, X. Xu. Y. Gu, Z. Dai, X. Cheng, J. Zhou,‡ Y. Jiang, T. Fan, J. Xu, *ACS Photonics*, **2019**, *6*, 1674.

[27] P. Günter, *Nonlinear Optical Effects and Materials*, Springer, Berlin, Germany **2000**, ch. 3.

[28] S. Kannan, A. Sekar, K. Sivaperuman, *J. Mater. Chem. C* **2020**, *8*, 16668.

[29] X. Liu, Z. Yang, D. Wang, H. Cao, *Crystals* **2016**, *6*, 158.

[30] S. H. Lee, B. J. Kang, B. W. Yoo, S. C. Lee, S. J. Lee, M. Jazbinsek, H. Yun, F. Rotermund, O. P. Kwon, *Adv. Funct. Mater.* **2017**, *27*, 1605583.

[31] J. Kim, Y. C. Park, J. H. Seok, M. Jazbinsek, O. P. Kwon, *Adv. Opt. Mater.* **2021**, *9*, 2001521.

[32] P. D. Cunningham, L. M. Hayden, *Opt. Express* **2010**, *18*, 23620.

[33] S. Saito, T. M. Inerbaev, H. Mizuseki, N. Igarashi, R. Note, Y. Kawazoe, *Chem. Phys. Lett.* **2006**, *432*, 157.

[34] A. M. S. Riel, R. K. Rowe, E. N. Ho, A. C. C. Carlsson, A. K. Rappé, O. B. Berryman, P. S. Ho, *Acc. Chem. Res.* **2019**, *52*, 2870.

[35] L. C. Gilday, S. W. Robinson, T. A. Barendt, M. J. Langton, B. R. Mullaney, P. D. Beer, *Chem. Rev.* **2015**, *115*, 7118.

[36] S. Kurtz, T. Perry, *J. Appl. Phys.* **1968**, *39*, 3798.

[37] I. Aramburu, J. Ortega, C. L. Folcia, J. Etxebarria, *Appl. Phys. Lett.* **2014**, *104*, 071107.

[38] S. J. Kwon, O. P. Kwon, J. I. Seo, M. Jazbinsek, L. Mutter, V. Gramlich, Y. S. Lee, H. Yun, P. Günter, *J. Phys. Chem. C*. **2008**, *112*, 7846.

[39] P. J. Kim, J. H. Jeong, M. Jazbinsek, S. J. Kwon, H. Yun, J. T. Kim, Y. S. Lee, I. H. Baek, F. Rotermund, P. Günter, O. P. Kwon, *CrystEngComm* **2011**, *13*, 444.

[40] M. A. Spackman, J. J. McKinnon, *CrystEngComm* **2002**, *4*, 378.

[41] J. J. McKinnon, D. Jayatilaka, M. A. Spackman, *Chem. Commun*. **2007**, *37*, 3814.

[42] M. A. Spackman, D. Jayatilaka, *CrystEngComm* **2009**, *11*, 19.

[43] Mercury 4.3.0 program, Cambridge Crystallographic Data Centre (CCDC), httpswww.ccdc.cam.ac.uk.

[44] J. H. Seok, U. Puc, S. J. Kim, W. Yoon, H. Yun, I. C. Yu, F. Rotermund, M. Jazbinsek, O. P. Kwon, *Adv. Opt. Mater.* **2021**, *9*, 2100618.

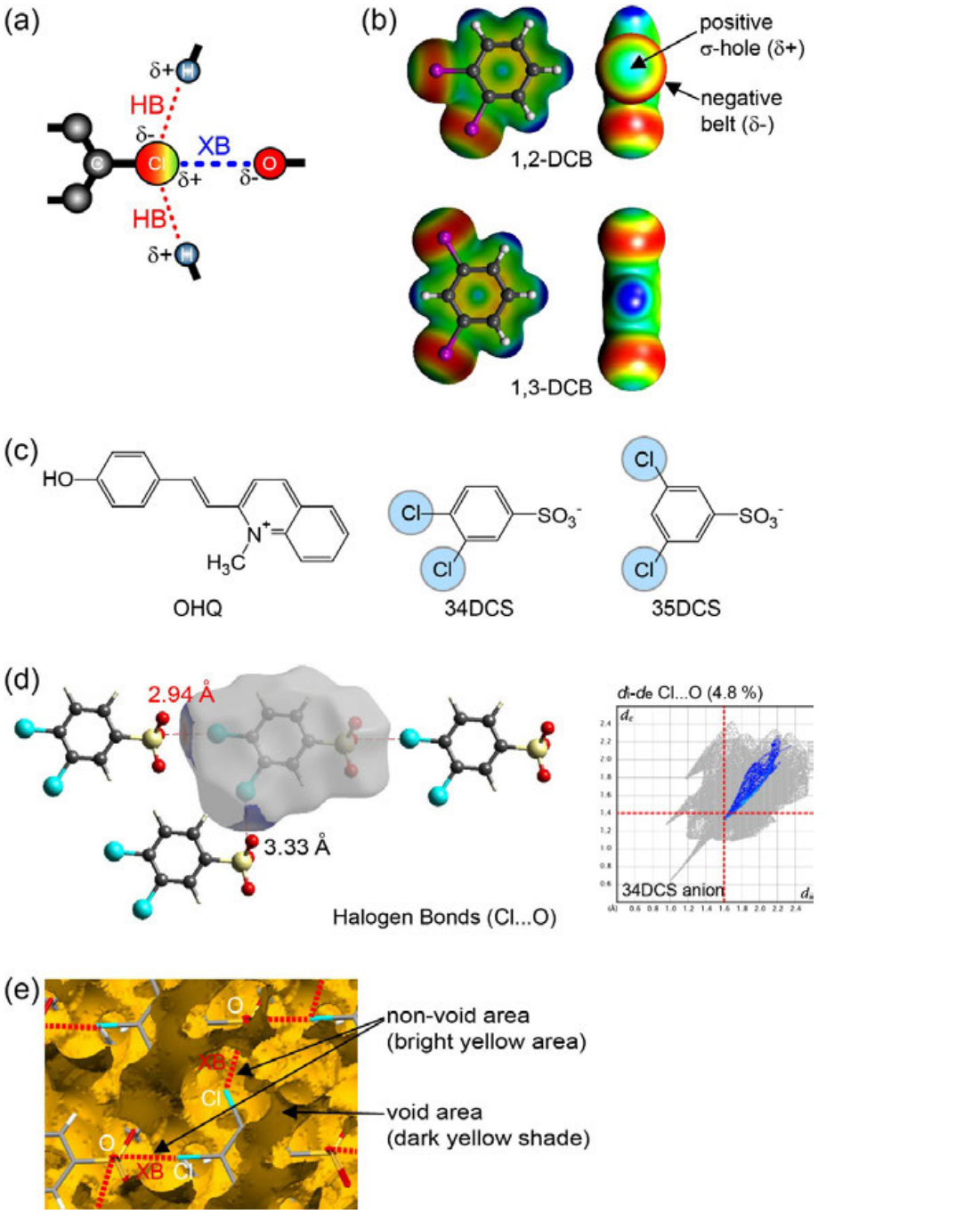

Figure 1. (a) Multi-intermolecular interaction ability of halogen (Cl) substituent with coexisting σ-hole (δ+) and negative belt (δ−) that can simultaneously form hydrogen bonds (HBs) and halogen bonds (XBs). (b) Electrostatic potentials of 1,2- and 1,3-dichlorobenezenes (DCB). (c) Chemical structure of non-centrosymmetric OHQ-34DCS and centrosymmetric OHQ-35DCS crystals. (d) XBs ((Ar)–Cl···$^{-}$O$_3$–S) of Cl substituents on 34DCS anion in OHQ-34DCS crystals presented with the Hirshfeld surface. (e) A part of the void shape around the 34DCS anion in OHQ-34DCS crystals. The red dotted lines are corresponding to XBs ((Ar)–Cl···$^{-}$O$_3$–S) in Figure 1d.

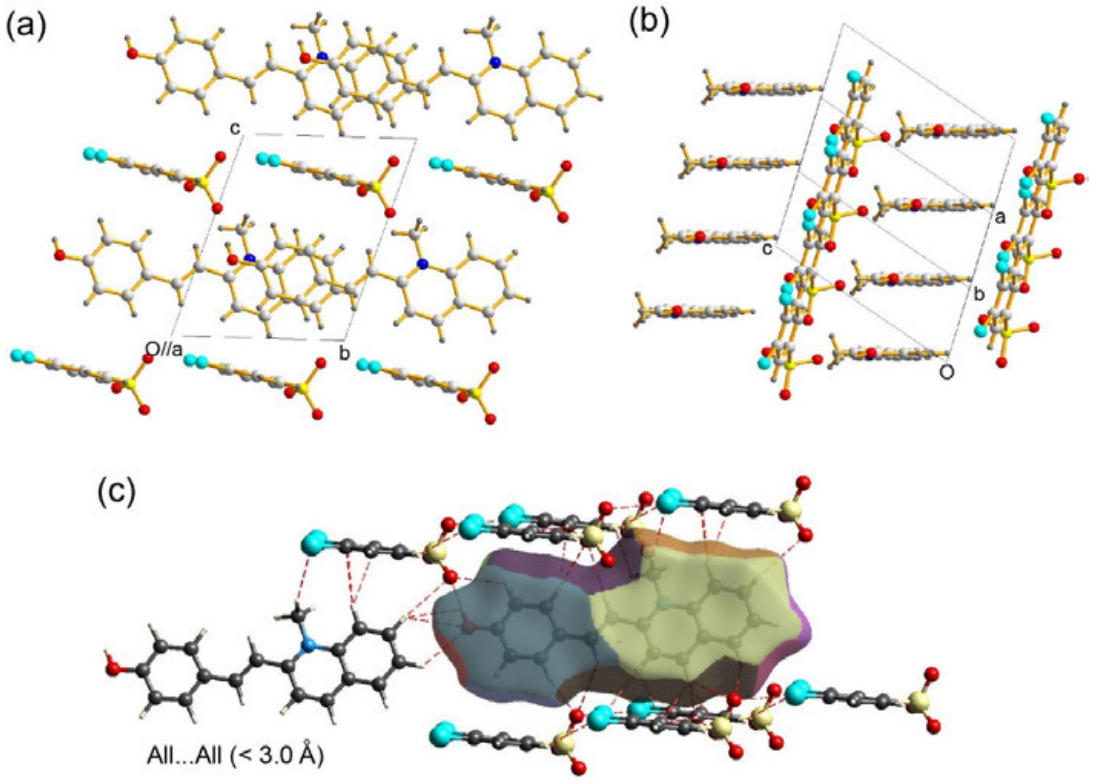

Figure 2. Molecular alignment in OHQ-34DCS crystals. (c) Hirshfeld surface analysis with fragment patch of OHQ cation in OHQ-34DCS crystals. The red dotted lines indicate the all···all atom contacts (< 3.0 Å).

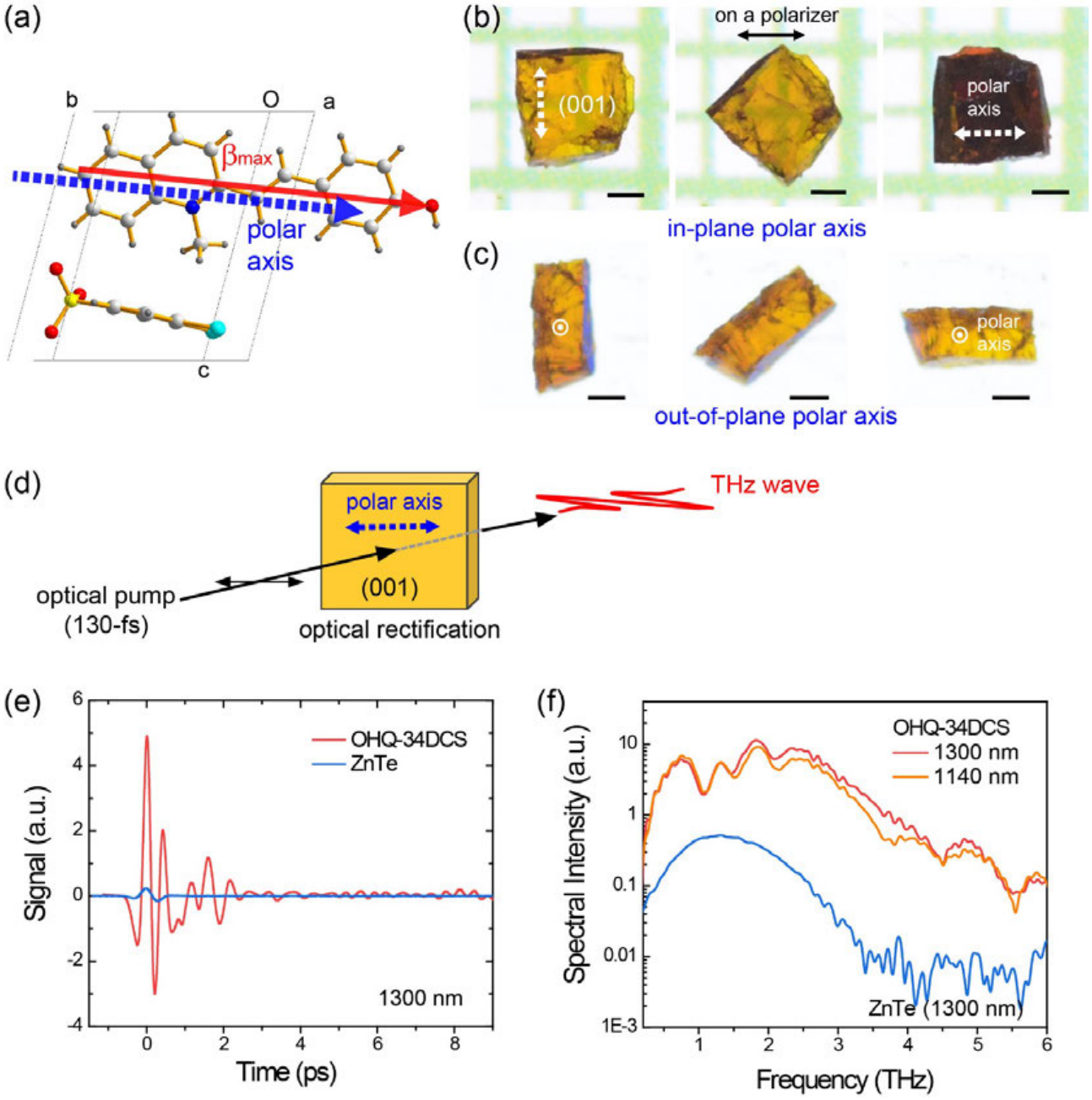

Figure 3. (a) Parallel alignment of the first hyperpolarizability β_{max} of OHQ chromophore with the polar axis of the OHQ-34DCS crystals. Photographs of OHQ-34DCS crystals with (b) in-plane and (c) (close-to) out-of-plane polar axes, taken in transmission with rotating the crystals on a polarizer (scale bar: 0.5 mm). (d) THz wave generation geometry (Figure S4). The double arrow presents the direction of light polarization (horizontal direction). THz wave generation in a 0.48-mm-thick OHQ-34DCS crystal and a 1.0-mm-thick ZnTe crystal: (e) time-domain signals at 1300 nm pump wavelength and (f) frequency domain signals at 1140 and 1300 nm pump wavelengths.

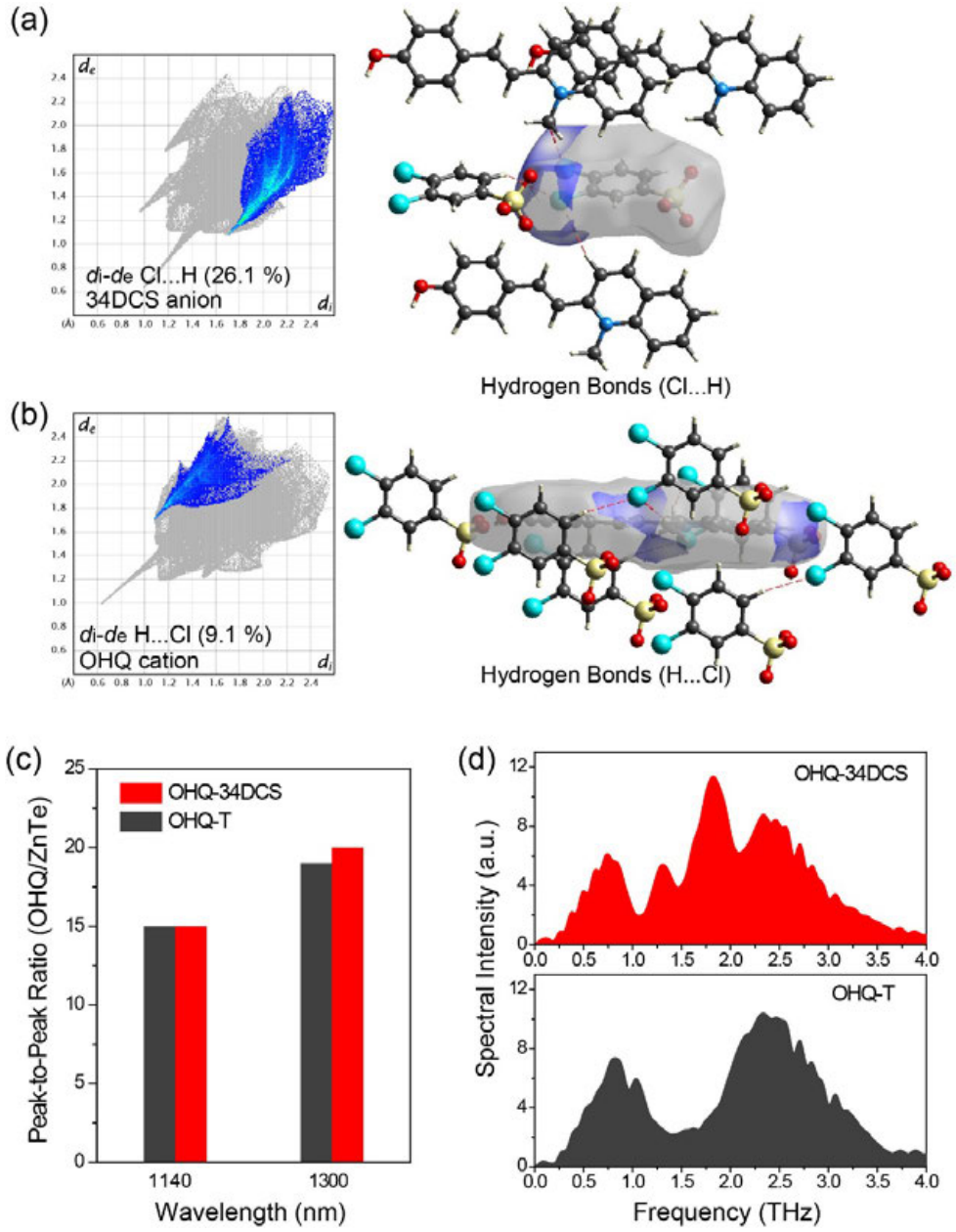

Figure 4. Intermolecular interactions of OHQ-34DCS crystals, presented with Hirshfeld surfaces of (a) 34DCS anion and (b) OHQ cation to show HBs between Cl and H. The red dotted lines indicate close contact (< 3.0 Å) of Cl···H and H···Cl. Note that these interactions do not exist in non-chlorinated OHQ-T crystals. THz wave generation results in a 0.48-mm-thick OHQ-34DCS crystal with *P1* space group and a 0.46-mm-thick OHQ-T crystal with *Pn* space group: (c) peak-to-peak ratio of the generated THz signal of these OHQ crystals relative to 1.0-mm-thick ZnTe crystal pumped at 1140 and 1300 nm and (d) frequency spectra for crystal pumped at 1300 nm.

Table of Contents

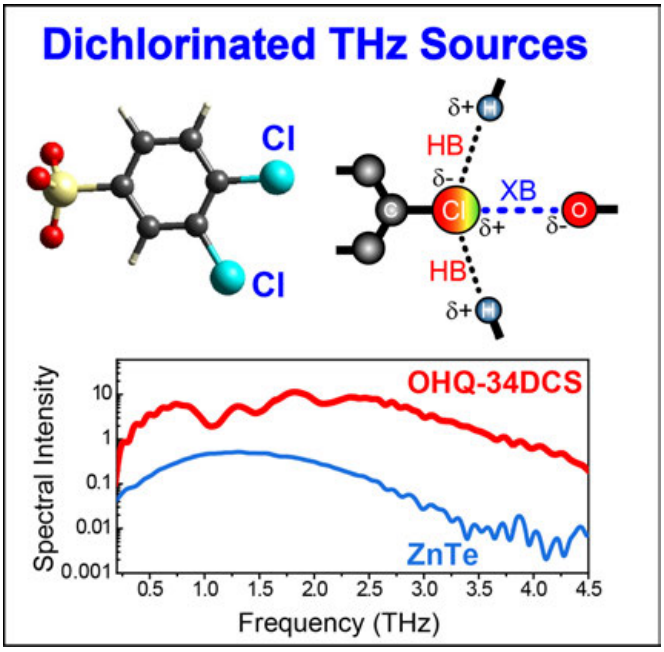

Organic-salt terahertz sources, that utilize dichlorinated aromatic molecular anions for the first time to the best of our knowledge, exhibit state-of-the-art optical-to-THz conversion efficiency and a flat spectral shape. In newly designed highly efficient nonlinear optical organic crystals, the dichlorinated groups form strong halogen bonds as well as hydrogen bonds that are beneficial for reducing self-absorption of terahertz source crystals.

Supporting Information

Dichlorinated Organic-Salt Terahertz Sources for THz Spectroscopy

Bong-Rim Shin†, *In Cheol Yu*†, *Mojca Jazbinsek, Woojin Yoon, Hoseop Yun, Sang-Wook Kim, Dongwook Kim, Fabian Rotermund*, O-Pil Kwon**

((Optional Dedication))

B. R. Shin, Prof. S. W. Kim, Prof. O. P. Kwon
Department of Molecular Science and Technology, Ajou University, Suwon 16499 (Korea)
E-mail: opilkwon@ajou.ac.kr
I. C. Yu, Prof. F. Rotermund
Department of Physics, Korea Advanced Institute of Science and Technology (KAIST), Daejeon 34141 (Korea)
E-mail: rotermund@kaist.ac.kr
Dr. M. Jazbinsek
Institute of Computational Physics, Zurich University of Applied Sciences (ZHAW), 8401 Winterthur (Switzerland)
W. Yoon, Prof. H. Yun
Department of Chemistry & Department of Energy Systems Research, Ajou University, Suwon 16499 (Korea)
Prof. D. Kim
Department of Chemistry, Kyonggi University, San 94-6, Iui-dong, Yeongtong-gu, Suwonsi, Gyeonggi 443-760 (Korea)

†These authors equally contributed to this work.

Keywords: terahertz waves; self-assembly, organic crystals; nonlinear optics; halogen bonds

A. Multi-Intermolecular Interactions

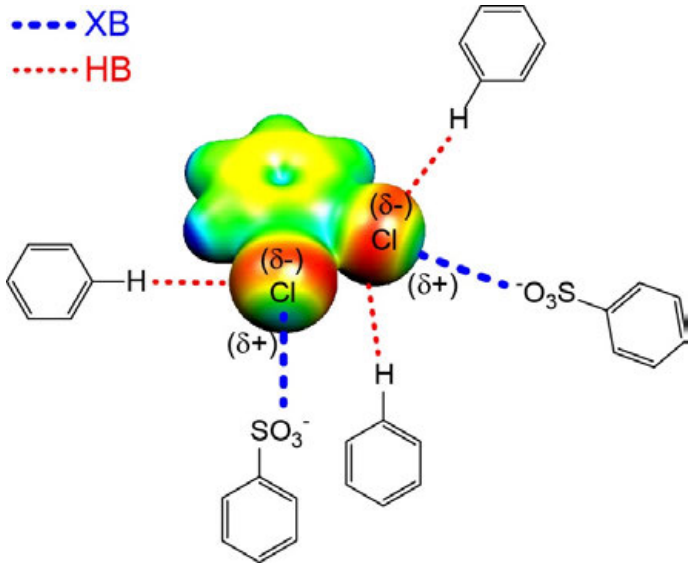

Figure S1. Example of possible multi-intermolecular interactions (halogen bonds, XBs and hydrogen bonds, HBs) of dichlorinated substituents on 1,2-dichlorobenzenes (Figure 1b) with other substituents commonly used in organic THz source crystals. These multi-intermolecular interactions can be also observed in OHQ-34DCS crystals, presented in Figure 1d for XBs and Figure 4a and 4b for HBs.

B. Synthesis

For OHQ-34DCS and OHQ-35DCS, the intermediates 1,2-dimethylquinolin-1-ium 3,4-dichlorobenzenesulfonate (MQ1-34DCS) and 1,2-dimethylquinolin-1-ium 3,5-dichlorobenzenesulfonate (MQ1-35DCS) were synthesized in a manner similar to that in the literature. [*Adv. Funct. Mater*., **2012**, *22*, 200] OHQ-34DCS and OHQ-35DCS were synthesized by a reaction with 4-hydroxybenzaldehyde and the corresponding intermediates. [*Adv. Funct. Mater*., **2012**, *22*, 200 and *Adv. Opt. Mater*. **2015**, *3*, 756]

1,2-dimethylquinolin-1-ium 3,4-dichlorobenzenesulfonate (MQ1-34DCS): Yield 89 %. ^{1}H NMR (600 MHz, DMSO-d_6, δ): 9.09 (d, 1H, J = 8.4 Hz, $C_{11}H_{12}N$), 8.59 (d, 1H, J = 8.4 Hz, $C_{11}H_{12}N$), 8.40 (d, 1H, J = 7.8 Hz, $C_{11}H_{12}N$), 8.23 (t, 1H, J = 7.8 Hz, $C_{11}H_{12}N$), 8.11 (d, 1H, J = 9 Hz, $C_{11}H_{12}N$), 7.99 (t, 2H, J = 7.2 Hz, $C_{11}H_{12}N$), 7.70 (s, 1H, $C_6H_3Cl_2SO_3^-$), 7.60 (d, 1H, J = 8.4 Hz, $C_6H_3Cl_2SO_3^-$), 7.53 (d, 1H, J = 6 Hz, $C_6H_3Cl_2SO_3^-$), 4.44 (s, 3H, NCH_3), 3.07 (s, 3H, $C_{11}H_{12}N$). ^{13}C NMR (DMSO-d_6, δ): 161.15, 148.82, 145.39, 139.15, 135.00, 130.96, 130.34, 130.29, 130.20, 128.93, 127.74, 127.34, 125.78, 125.09, 118.92, 22.98. Elemental analysis of $C_{17}H_{15}Cl_2NO_3S$: calc'd. C 53.13, H 3.93, Cl 18.45, N 3.64, O 12.49, S 8.34; found: C 53.36, H 3.86, N 3.66, S 8.39.

1,2-dimethylquinolin-1-ium 3,5-dichlorobenzenesulfonate (MQ1-35DCS): Yield 86 %. ^{1}H NMR (600 MHz, DMSO-d_6, δ): 9.09 (d, 1H, J = 8.4 Hz, $C_{11}H_{12}N$), 8.59 (d, 1H, J = 9 Hz, $C_{11}H_{12}N$), 8.40 (d, 1H, J = 7.2 Hz, $C_{11}H_{12}N$), 8.23 (t, 1H, J = 8.4 Hz, $C_{11}H_{12}N$), 8.11 (d, 1H, J = 7.8 Hz, $C_{11}H_{12}N$), 7.99 (t, 2H, J = 7.8 Hz, $C_{11}H_{12}N$), 7.58 (s, 1H, $C_6H_3Cl_2SO_3^-$), 7.50 (s, 2H, $C_6H_3Cl_2SO_3^-$), 4.44 (s, 3H, NCH_3), 3.07 (s, 3H, $C_{11}H_{12}N$). ^{13}C NMR (DMSO-d_6, δ): 161.15, 151.55, 145.41, 139.17, 135.02, 133.55, 130.30, 128.95, 127.97, 127.76, 125.09, 124.18, 118.93, 22.98. Elemental analysis of $C_{17}H_{15}Cl_2NO_3S$: calc'd. C 53.13, H 3.93, Cl 18.45, N 3.64, O 12.49, S 8.34; found: C 53.25, H 3.86, N 3.65, S 8.33.

2-(4-hydroxystyryl)-1-methylquinolin-1-ium 3,4-dichlorobenzenesulfonate (OHQ-34DCS): Yield = 61 %. ^{1}H NMR (600 MHz, DMSO-d_6, δ): 10.41 (s, 1H, OH), 8.97 (d, 1H, J = 9 Hz, $C_{11}H_{12}N$), 8.53 (m, 2H, $C_{11}H_{12}N$), 8.32 (d, 1H, J = 8.1 Hz, $C_{11}H_{12}N$), 8.21 (d, 1H, J = 15.6 Hz, C_2H_2), 8.15 (t,

1H, *J* = 8.1 Hz, $C_{11}H_{12}N$), 7.92 (t, 1H, *J* = 7.2 Hz, $C_{11}H_{12}N$), 7.87 (d, 2H, *J* = 9 Hz, C_6H_4), 7.71 (m, 2H, C_2H_2, $C_6H_3Cl_2SO_3^-$), 7.60 (d, 1H, *J* = 7.8 Hz, $C_6H_3Cl_2SO_3^-$), 7.53 (d, 1H, *J* = 8.1 Hz, $C_6H_3Cl_2SO_3^-$), 6.93 (d, 2H, *J* = 9 Hz, C_6H_4), 4.52 (s, 3H, NCH_3) ^{13}C NMR (DMSO-d_6, δ): 161.23, 126.43, 148.80, 147.79, 143.31, 139.14, 134.60, 131.76, 131.06, 130.42, 130.27, 129.97, 128.61, 127.44, 127.38, 126.23, 125.86, 120.66, 119.14, 116.34, 115.36. Elemental analysis of $C_{24}H_{19}Cl_2NO_4S$: calc'd. C 59.02, H 3.92, Cl 14.52, N 2.87, O 13.10, S 6.57; found: C 59.07, H 3.99, N 2.87, S 6.69.

2-(4-hydroxystyryl)-1-methylquinolin-1-ium 3,5-dichlorobenzenesulfonate (OHQ-35DCS): Yield = 52 %. ^{1}H NMR (600 MHz, DMSO-d_6, δ): 10.40 (s, 1H, OH), 8.97 (d, 1H, *J* = 9 Hz, $C_{11}H_{12}N$), 8.53 (m, 2H, $C_{11}H_{12}N$), 8.31 (d, 1H, *J* = 8.1 Hz, $C_{11}H_{12}N$), 8.20 (d, 1H, *J* = 16.2 Hz, C_2H_2), 8.15 (t, 1H, *J* = 8.4 Hz, $C_{11}H_{12}N$), 7.92 (t, 1H, *J* = 7.8 Hz, $C_{11}H_{12}N$), 7.87 (d, 2H, *J* = 7.8 Hz, C_6H_4), 7.71 (d, 1H, *J* = 15.6 Hz, C_2H_2), 7.57 (s, 1H, $C_6H_3Cl_2SO_3^-$), 7.50 (s, 2H, $C_6H_3Cl_2SO_3^-$), 6.93 (d, 2H, *J* = 9 Hz, C_6H_4), 4.52 (s, 3H, NCH_3) ^{13}C NMR (DMSO-d_6, δ): 161.25, 156.49, 151.43, 147.81, 143.39, 139.18, 134.67, 133.71, 131.81, 130.03, 128.68, 128.17, 127.43, 126.28, 124.30, 120.70, 199.17, 116.20, 115.40. Elemental analysis of $C_{24}H_{19}Cl_2NO_4S$: calc'd. C 59.02, H 3.92, Cl 14.52, N 2.87, O 13.10, S 6.57; found: C 59.63, H 3.84, N 2.90, S 6.52.

C. Physical Properties

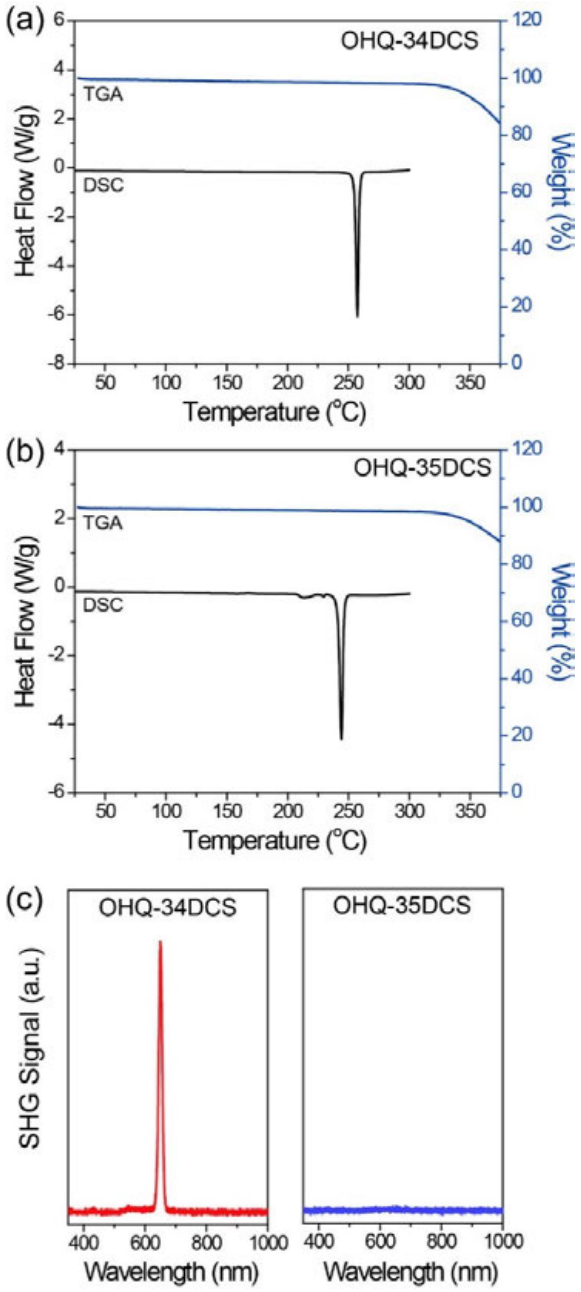

Figure S2. TGA and DSC thermodiagrams of (a) OHQ-34DCS and (b) OHQ-35DCS. (c) Powder SHG measurements of OHQ-34DCS and OHQ-35DCS. The fundamental wavelength is 1300 nm.

D. Crystal Structure Analysis

OHQ-34DCS: $C_{18}H_{16}NO \cdot C_6H_3Cl_2O_3S$, M_r = 488.36, triclinic, space group *P*1, a = 7.4737(3) Å, b = 8.1133(3) Å, c = 10.0214(5) Å, α = 69.592(1)°, β = 77.186(1)°, γ = 76.676(1)°, V = 547.49(4) Å^3, Z = 1, T = 290(1) K, μ(MoKα)= 0.43 mm^{-1}. Of 5410 reflections collected in the θ range 3.3-27.5° using ω scans on a Rigaku R-axis Rapid S diffractometer, 4084 were unique reflections (R_{int} = 0.015). The structure was solved and refined against F^2 using SHELXL-2018/3, [G. M. Sheldrick, Acta Cryst. C71, **2015**, 3] 291 variables, wR_2 = 0.085, R_1 = 0.030 ($F_o^2 > 2\sigma(F_o^2)$), GOF = 1.09, and max/min residual electron density 0.22/-0.23 eÅ^{-3}. CCDC- 2128133.

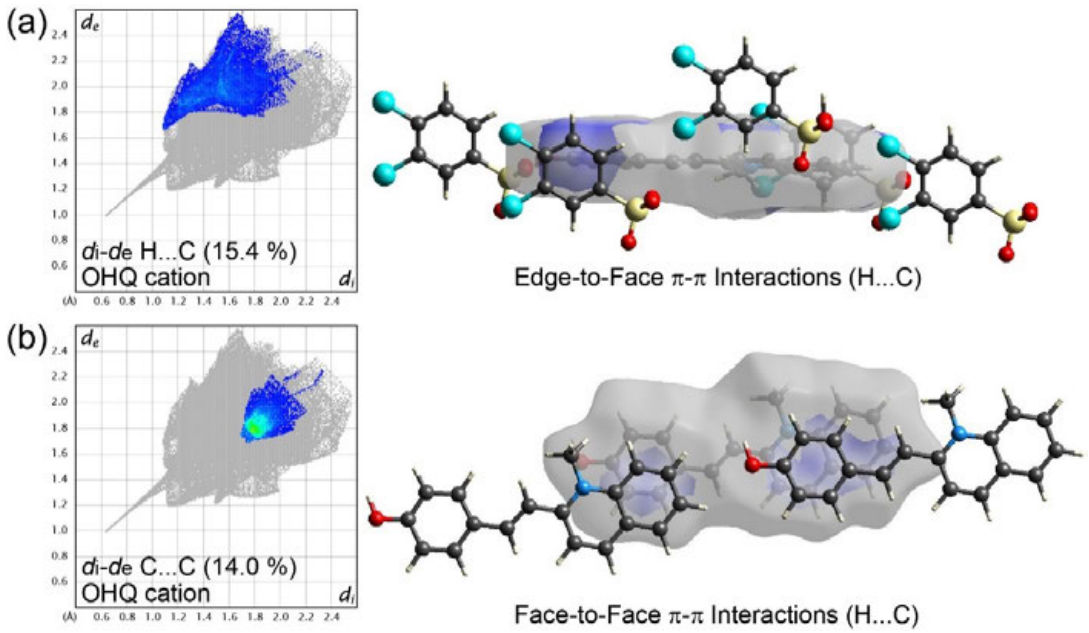

Figure S3. Intermolecular interactions of OHQ-34DCS crystals, presented with Hirshfeld surfaces of the OHQ cation to show (a) edge-to-face interactions with the atom contact of H···C and (b) face-to-face π-π interactions with the atom contact of C···C.

E. Optical Nonlinearity

For evaluating the microscopic and the macroscopic optical nonlinearity for OHQ-34DCS single crystals, the components of the first hyperpolarizability tensor β_{ijk} of OHQ cation possessing the experimental conformation (EXP) in the crystal structure of OHQ-34DCS crystals were calculated by density functional theory (DFT) calculations at the B3LYP/6-311+G(d,p) level according to Ref. [*J. Phys. Chem. C* **2008**, *112,* 7846; *CrystEngComm*, **2011**, *13*, 444]. The corresponding maximum first hyperpolarizability β_{max} of OHQ (EXP) cation along the main charge-transfer direction (very close to the direction *x* in DFT calculations) was also calculated. The results for OHQ-34DCS crystals are listed in Table S1.

Table S1. Molecular optical nonlinearity of OHQ-34DCS crystals: the components of the first hyperpolarizability tensor β_{ijk} ($\times 10^{-30}$ esu) and the corresponding maximum first hyperpolarizability β_{max} of OHQ cation possessing the experimental conformation (EXP) in OHQ-34DCS crystals.

	OHQ (EXP)
β_{xxx}	118.4
β_{xxy}	-7.8
β_{xyy}	-1.8
β_{yyy}	0.2
β_{xxz}	-0.3
β_{xyz}	-0.1
β_{yyz}	0
β_{xzz}	0.6
β_{yzz}	0
β_{zzz}	0
β_{max}	119.1

The ordering angle θ_p between the directions of the maximum first hyperpolarizability β_{max} of OHQ (EXP) cation and the polar axis in OHQ-34DCS crystals is zero due to the *P1* space group symmetry consisting of only one OHQ cation in the unit cell in OHQ-34DCS crystals. Consequently,

the order parameter of OHQ-34DCS crystals is maximum possible ($\cos^3\theta_p$ = 1.0) with all chromophores perfectly parallel. The value of the largest diagonal component of the effective first hyperpolarizability for the OHQ-34DCS crystal is according to the oriented gas model [*Phys. Rev. A* **1982**, 26, 2028] identical with that of maximum first hyperpolarizability β_{max} of OHQ (EXP) cation; $\beta_{111}^{eff} = \beta_{max} = 119 \times 10^{-30}$ esu.

F. Experiments on THz Wave Generation

S)8!'6.! .b&.8(<.*'!)*! .99(0(.*'!@YV!=+F.! A.*.8+'()*#!=*!%YdLTI-Q5! 08BG'+,,)('6! +*!(*L&,+*.!
&),+8!=b(G!=+G!&?<&./! WB'T[L9GG!&'(0+,!&?,G.G#6(06!=.8.! A.*.8+'./! 98)<!+*!)&'(0+,!&+8+<.'8(0!
+<&,(9(.83@%7C57!8(<.LS#5&.0'8+,!76BG(0G!&?<&./!WB!'LNYV!8!A.*.8+'(F.!@(MG+&&&6(8.!(9(.8!
$5&('9(8.78)#!5&.0'8+,!76BG(0G1@!6.!(*0(/.*'! +*A,.!)9! '6.!)&'(0+,!&?<&!=+G!*)8<+,! ')! '6.!
08BG'+,,)A8+&&8[0!'1!&,+*.)9!'6.! %YdLTI-Q5! 08BG'+,,#6(,.! &?<&!=+F.,.*A'6G!)9!""I[! +*/!"T[[!
*<! =.8.! ?G./! 9)8!0)<&+8(G)*3!8)8!/.'.0'()*)9!'6.! A.*.8+'./! @YV!=+F.G#!,.0'8)L)&'(0!G+<&,(*A!
$K%51!=+G0+88(./)?'! (*!=[3TL<<L'6(0N!h""[g!]+7! 08BG'+,,)('6! "[[L9GG+<&,(*A&?,G.G!'Z[[! *<!
A.*.8+'./!98)<!'6.!G+<.!@(MG+&&&6(8.!+<&,(9(.83!@6.!.b&.8(!G*?&!(G!G6)=*!(*!S(A?8.!5I3

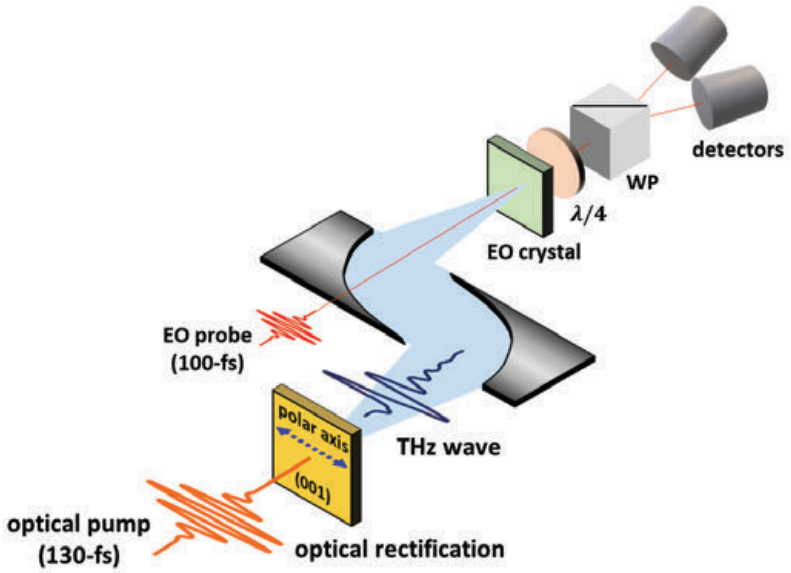

Figure S43!506.<+'(0!)9!@YV!=+F.!A.*.8+'()*!A.)<.'8B3

@6.!@YVL9(.,/!G'8.*A'6!+G!.+G?8./! +G!9?*0'()*!)9!'6.!)&'(0+,&?<&&)=.8!(*!'6.! &)=.8!,.F.,!98)<!H!')!"Z!<:3!@6.G.!8.G?,'G!+8.!G6)=*!(*!S(A?8.!5c3

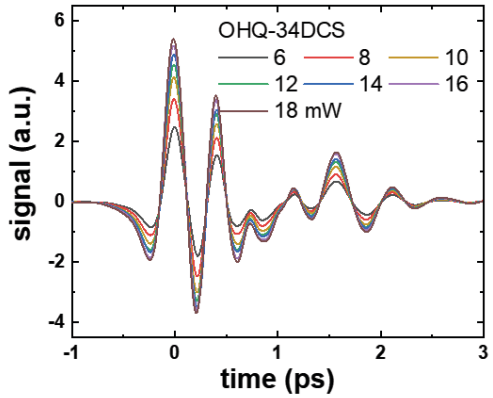

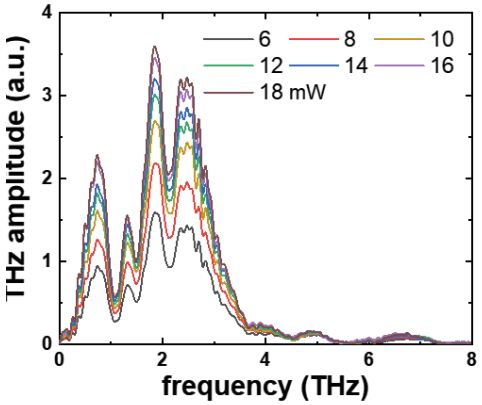

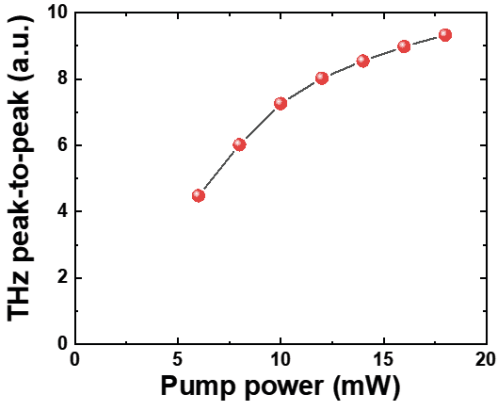

F)*3!$+1!].*.8+'./!@YV!=+F.G!(*!'(<.!)<+(*!+*/ $W1!98._?.*0B!/)<+(*3!$01!7?<&L&)=.8!/.&.*/.*0.!)9!&.+NL&)LN!@YV!9(.,/!G'8.*A'63

G. THz Absorbance Measurement

C!8.9.8.*0.! @YV=!+F.! (GA.*.8+'./! 98)<!7>^Q,dL@#!=6(06!.b6(W('G-!W8)+/W+*@YVG&.0'8?<! 98)<![!')! ^!@YV@6.!+WG)8&'()G&.0'8?<)9!%YdLTI-Q5! 08BG'+(,G0+,0?,+'./! WB!)<&+8(*A6.! @YV=!+F.! &+GG(*A8)?A6!'6.! 08BG'+=!('6! '6.! 8.9.8.*0.! @YV=!+F.3!@6.!<.+G?8./! +WG)8W+*(G! /(G&,+B./!+,)*A!=('6 +/B*+<(0!8+*A.(*/(0+'(*A!6.! ,(<(!')9!)?8!+WG)8W+*0.!G?8.<.*'! GBG'.<(*! S(A?8.!5H3

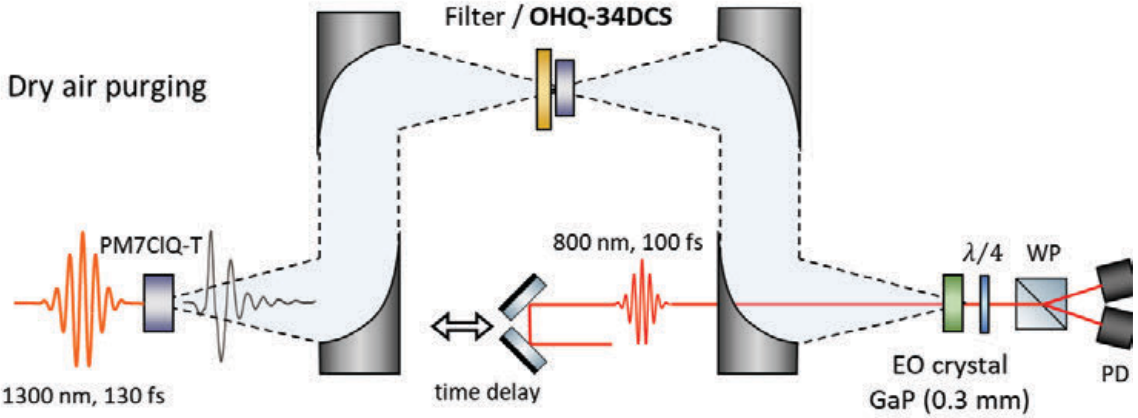

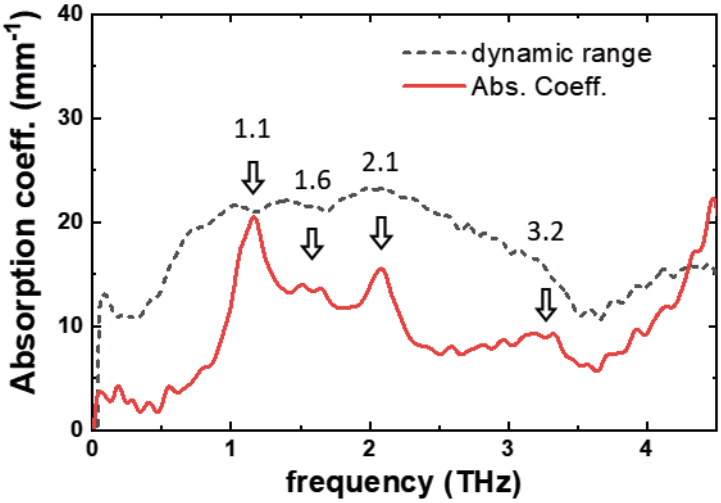

Figure S6 3!$+15 06.<+'(0!)9!+WG)8W+*0.!G?8.<.*'! (*!'6.! @YV9 8._?.*0B!8+*A.!=*/! $W16.! <.+G?8./!+WG)8W+*0.!)9!+![3IZL<<L'6(0N!%YdLTI-Q5!08BG'+,3